Applied Surface Science 258 (2012) 3227–3231

Contents lists available at SciVerse ScienceDirect

Applied Surface Science

journal homepage: www.elsevier.com/locate/apsusc

In situ measurement of the kinetic friction of ZnO nanowires inside a scanning electron microscope

Boris Polyakov[a,b,*], Leonid M Dorogin[a], Ants Lohmus[a], Alexey E Romanov[a,c], Rynno Lohmus[a]

[a] Institute of Physics, University of Tartu, Riia st. 142, Tartu, Estonia
[b] Institute of Solid State Physics, University of Latvia, Kengaraga st. 8, Riga, Latvia
[c] Ioffe Physical Technical Institute, RAS, Politehnicheskaja st. 26, St. Petersburg, Russia

ARTICLE INFO

Article history:
Received 28 June 2011
Received in revised form 31 October 2011
Accepted 15 November 2011
Available online 25 November 2011

Keywords:
Nanotribology
SEM
Nanowire
Zinc oxide
Graphite
Silicon

ABSTRACT

A novel method for measuring the kinetic friction force in situ was developed for zinc oxide nanowires on highly oriented pyrolytic graphite and oxidised silicon wafers. The experiments were performed inside a scanning electron microscope and used a nanomanipulation device as an actuator, which also had an atomic force microscope tip attached to it as a probe. A simple model based on the Timoshenko elastic beam theory was applied to interpret the elastic deformation of a sliding nanowire (NW) and to determine the distributed kinetic friction force.

1. Introduction

Semiconducting nanowires have been the focus of intense research during the past few decades [1,2]. In particular, much experimental data regarding nanowire (NW) mechanical properties have accumulated [3–5]. However, few of them are related to NW-substrate friction and shear strength on a flat substrate. Detailed understanding of interfacial phenomena, such as friction and shear strength, are equally important among an array of other mechanical properties (Young's modulus, ultimate strength, etc.) for the nanomanipulation and engineering of NW based electronic, electromechanical and photonic nanodevices. NW friction on flat substrates is strong enough to balance highly deformed NWs in bend state, producing high strain, which is especially important for piezoresistive or/and piezoelectric materials such as Si or ZnO [6].

Desai and Haque described the bending of ZnO NWs attached to a transmission electron microscope grid and the friction properties of NWs sliding along the front edge of an atomic force microscope (AFM) cantilever [7]. Zhu et al. investigated the buckling and tip contact friction of a ZnO NW that was welded to a tungsten tip and rested against a gold substrate by its free end [8]. For the studies described above, the friction was considered across a small contact area between the NW and the substrate.

The friction of a full-length NW on a substrate was presented by the following authors. Manoharan et al. performed a study that examined the ZnO NW mechanical properties [9] and NW-substrate adhesion and friction of long ZnO NWs on a silicon substrate [10]. They examined the friction force during the dragging of a NW (parallel to its axis) at various loadings. This work describes the only available data in the literature regarding the interfacial shear strength for full-length ZnO nanowires on a flat substrate. Wong et al. reported a method for simultaneous measuring the friction, elastic forces and ultimate strength of SiC NWs [11]. SiC NWs and carbon nanotubes were deposited on a MoS_2 substrate and pinned on one end by square metallic pads that were evaporated through a shadow mask. The free ends of the nanowires were contacted by an AFM tip, and the lateral forces were recorded. Bordag et al. introduced a simple method for determining the friction force of InAs NWs on Si_3N_4-coated silicon wafers that was based on measuring the ultimate NW bending radius of curvature after manipulation, which results from a balance between friction and elastic forces [12,13]. However, their model neglects the role of NW free ends, which may significantly influence the results [14].

Most of the friction measurements on nanotubes and NWs were performed using a conventional AFM at ambient conditions [11,12,15,16]. An AFM allows a high level of control of the applied force and extremely precise manipulation. However, it has several limitations. An AFM can be used either for visualisation (raster

* Corresponding author at: Institute of Physics, University of Tartu, Riia st. 142, Tartu, Estonia.
E-mail addresses: boriss.polakovs@ut.ee, celbic@yahoo.com (B. Polyakov).

0169-4332/$ – see front matter © 2011 Elsevier B.V. All rights reserved.
doi:10.1016/j.apsusc.2011.11.069

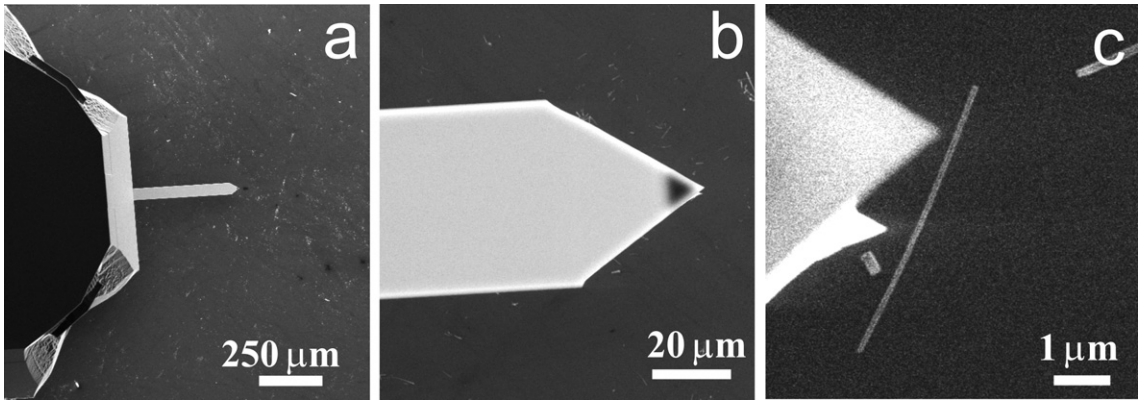

Fig. 1. SEM images of the AFM chip with the cantilever in contact with the sample. Top view.

scanning) or manipulation (line scan) of NWs. It is impossible to control the profile of a NW during its displacement, as well as the tip shape of the AFM.

In the present work, we describe a novel method for measuring distributed kinetic friction that involves in situ dragging of a ZnO NW perpendicular to its axis by an AFM tip inside a scanning electron microscope (SEM) chamber on an oxidised silicon wafer and highly oriented pyrolytic graphite (HOPG). We used SEM to visualise interactions between the tip and the NW, which enabled us to monitor evolution of the NW profile during manipulation, as well as any changes to the AFM tip geometry. Elastic deformation of a NW sliding on a substrate surface was used to determine the distributed kinetic friction force. Based on our knowledge, this work is the first to report utilisation of this method.

2. Experiment

The ZnO NW was chosen as a highly promising and well-studied material [17]; this also granted us the opportunity to compare the present results with data reported in the literature. ZnO NWs were grown using 60 nm Au nanoparticles (*BBI international*) as a catalyst for the vapor transport method [18]. NWs were grown on silicon substrates by heating a 1:4 mixture of ZnO and graphite powder to 800–900 °C in an open-ended quartz tube over a period of thirty minutes. Synthesised NWs were 10–20 μm long and had diameters in the range of 60–200 nm. After growth, the wires were removed from the substrate and transferred to a silicon substrate with a 50 nm thick SiO_2 layer (*Semiconductor Wafer, Inc.*) or to freshly cleaved HOPG (*SPI Supplies*). The transfer was carried out by mechanically wiping the wires from the initial substrate using a piece of cleanroom paper and then by placing them on the silicon wafer or HOPG surface.

Contact mode AFM cantilevers (*Nanosensor* AdvancedTEC-CONT cantilevers, force constant 0.02–0.75 N/m, nominal tip radius 10 nm) were used for NW manipulation. The manufacturer-labelled average value of the force constant $C = 0.2$ N/m was used for the force calculation. The AFM chip was mounted on a three-dimensional nanomanipulator equipped with position sensors (SLC-1720-S, *SmarAct*) and installed inside an electron microscope (*TESCAN Vega-II SBU*). The typical vacuum pressure in the chamber was 3×10^{-4} mbar. The nanomanipulator can be operated in either a step or scan regime. For the first regime, the nanomanipulator works as a stepping piezo motor (based on inertial sliding or the stick-slip effect). The second regime uses a continuous elongation of the piezo element at a value of approximately 1.4 μm.

We used AFM cantilevers, and their geometry enabled us to see the end of the tip from a top view at 10° cantilever-to-sample tilt (Figs. 1a–c, 3a). Tip-sample contact was detected visually as a sudden stabilisation of the tip vibration and the beginning of tip lateral sliding. The applied force F_{load} was defined as the normal force determined from the cantilever deflection Δz multiplied by its normal force constant C.

NW deposited on a silicon wafer or HOPG was pushed by AFM tip at gradually increasing vertical loading force until NW becomes displaced. Static friction force was estimated using cantilever deflection and NW-tip contact angle. Elastically deformed profile of NW dragged by tip at midpoint and Young modulus of NW were exploited for calculation of kinetic friction force. AFM cantilevers were used as probes, and no AFM feedback loop was used in the experiment. Nearly constant loading force was ensured by parallel to surface movement of nanomanipulator. All experiments were performed at room temperature.

3. Results and discussion

Short and rigid NWs slide (or rotate) as a whole object; this behaviour becomes more complicated for the case of long NWs. At the instant that the AFM cantilever tip contacts the NW, the static friction force q_{st} is distributed over a portion of the NW of unknown length l, which may be smaller than the entire NW length L (Fig. 2a). The NW becomes displaced by the tip only for its portion l' where the applied force exceeds the ultimate value of the distributed static friction force (corresponding to the maximum shear strength) (Fig. 2b). Static friction acts on the intact part of the NW of length $L - l'$, while kinetic friction affects the displaced portion l' of the NW. For a partially displaced NW, the effective friction force is the sum of the static q_{st} and kinetic q_{kin} friction forces. It is difficult to separate the contribution of the static and kinetic friction forces during the initial stage of NW displacement. We will refer to the combined distributed static and kinetic friction forces as q_{com}. However, we suppose that the value of the combined friction force is close to that of the pure static friction, which may be used as an approximate estimation of the static friction force. Upon further displacement of the NW (during uniform translation), we consider the friction force as purely kinetic and uniformly distributed along the length of the NW (Fig. 2c).

3.1. Combined friction

Once the tip contacts the sample surface, upon approach of the AFM chip towards the surface the tip slides easily across the surface. Low tip-substrate friction is provided by small friction coefficient [19] and small spring constant, and tilted geometry of cantilever respective to sample surface, which enables lateral sliding of the tip and prevents it from blocking and "slip-stick" behaviour. Let us imagine uniform movement of the tip along the substrate surface

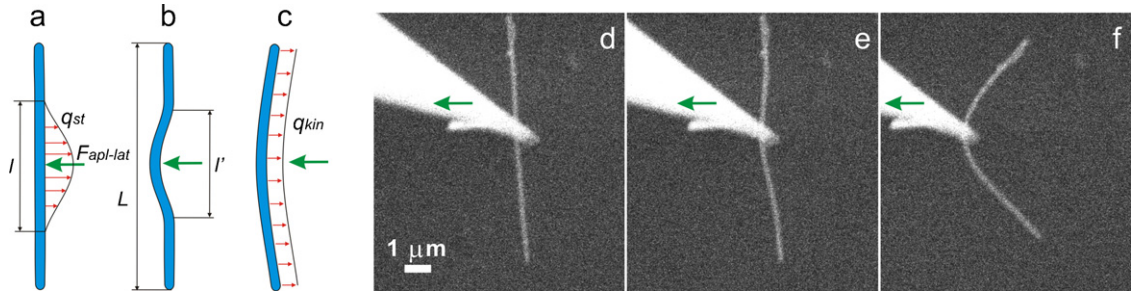

Fig. 2. Nanowire manipulation. Schematics: applied force $F_{apl\text{-}lat}$ and static friction force q_{st} (a). Partially displaced nanowire (b). Entirely displaced nanowire. Kinetic friction force q_{kin} equally distributed over NW length (c). SEM images of nanowire displacement; the arrows indicate the direction of tip movement (d, e, f).

at constant load. F_{load} is a force generated by elastic deformation of cantilever and directed perpendicular to the sample plane. The vector of the total applied force F_{apl} tilts from the normal direction due to kinetic friction force acting between the tip and the substrate (Fig. 3a). Once the tip contacts the NW, vertical component of the force applied by tip F_{load} becomes balanced by NW-substrate normal reaction force $F_{n\text{-}s}$, while tip-substrate friction force disappears (Fig. 3b). Lateral component of applied force $F_{apl\text{-}lat}$ opposes the NW-substrate static friction $F_{f\text{-}s}$.

The lateral component of the applied force $F_{apl\text{-}lat}$ can be expressed through the F_{load} and contact angle α [20,21]:

$$F_{apl-lat} = F_{load} \times ctg(\alpha). \quad (1)$$

Angle α is determined by the tip-nanowire contact geometry (Fig. 3b and e). The tip r_{tip} and NW radii r_{NW} were taken from SEM images in order to calculate the contact angle α for each measurement (Fig. 3e):

$$\alpha = \arcsin\left(\frac{r_{tip} - r_{NW}}{r_{tip} + r_{NW}}\right). \quad (2)$$

Some tips were rather brittle and the very tip breaks fast, when tip radius was equal to the radius of the NW $r_{tip} \approx r_{NW}$. However, tips become much more robust and do not change significantly, when tip radius becomes approximately two times bigger than NW radius $r_{tip} \approx 2r_{NW}$. It should be noted that the top view of an SEM image gives only an approximate estimation of the true AFM tip radius. To determine the true contact radius of the tip, it is necessary to observe the probe tip from the side view. Final tip shape was examined from the side view at the end of the experiment to confirm our estimations of tip radius from the top view.

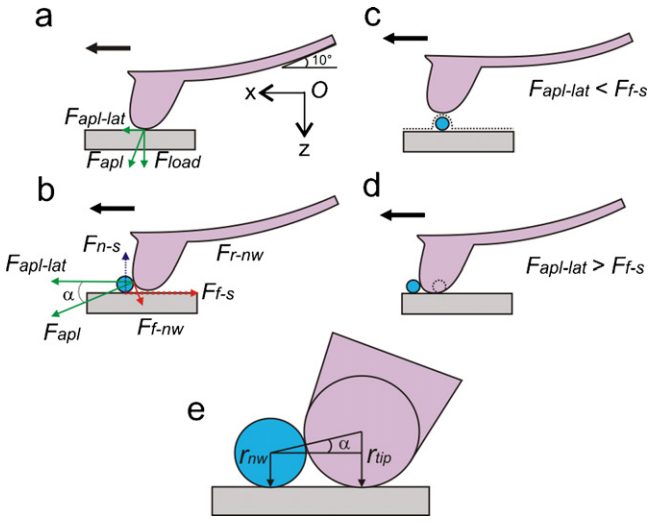

Fig. 3. Schematics of the combined friction measurement. The tip slides over a flat surface (a). The tip contacts the NW, producing a static friction force on the tip (b). Possible tip trajectory: the tip moves across the NW. The applied lateral force is less than the ultimate static friction force (c). Alternate trajectory: the tip displaces the NW. The applied lateral force is greater than the ultimate static friction force (d). Contact geometry of the tip and the NW (e).

There are several possible scenarios for the subsequent tip trajectory when it contacts a NW. If lateral component of applied force $F_{apl\text{-}lat}$ does not exceed NW-substrate ultimate static friction $F_{f\text{-}s}$, then the NW remains motionless and the tip slides across the NW (Fig. 3b and c). Friction between the tip and the NW $F_{f\text{-}NW}$ resist tip sliding across the NW. However, we observed that the tip-NW friction $F_{f\text{-}NW}$ was not strong enough to prevent the tip from sliding across the NW and to impede the lateral movement of the tip in most cases. Therefore, we will neglect tip-NW friction for the sake of simplicity.

Total force applied by tip F_{apl} causes momentum $M_{apl} = F_{apl} \times r_{NW} \times \cos(\alpha)$, which turns NW counter clockwise and produce torsion strain in the NW. Rotation of the NW facilitates sliding of tip across it. However, rotation of faceted NW is possible at condition of detachment of the NW from the substrate, which has low probability due to high NW-substrate adhesion forces.

The NW starts to move, when lateral component of force applied by tip $F_{apl\text{-}lat}$ exceeds the ultimate static friction force $F_{f\text{-}s}$ (Fig. 3b and d). Before that moment $F_{apl\text{-}lat} = F_{f\text{-}s}$. We monitored the NW for initial sliding at gradually increasing loading force F_{load} to estimate approximate ultimate static friction force $F_{f\text{-}s}$.

To obtain the average distributed friction force q_{com}, the measured friction force $F_{f\text{-}s}$ was divided by the NW length L. The friction force $F_{f\text{-}s}$ was measured for a set of 16 NWs on HOPG and 16 NWs on silicon. The NW diameter ranged from 60 to 160 nm (average diameter of 110 nm). We observed values of q_{com} in the range of 0.12–16 nN/nm on HOPG and of 0.04–7.5 nN/nm on silicon wafers.

Interfacial shear stress σ is considered to be a fundamental property of nanoscale friction $F_{friction} = \sigma A$, where A is the contact area [9,22]. Assuming a hexagonal cross section [18] $A = LD/\sqrt{3}$, where D is the NW diameter; thus, the average shear stress was found to be $\sigma_{com} = 24$ MPa on HOPG and $\sigma_{com} = 36$ MPa on silicon.

3.2. Kinetic friction

To exclude the effect of the tip radius and contact angle uncertainties, we have developed a method in which a NW profile analysis is used to determine the NW-substrate kinetic friction during translation. After manipulation, the NW profile is determined by balancing its elastic force with the NW-substrate distributed friction forces [11,12]. If the elastic force is much higher than the friction force, then the NW behaves as a straight, rigid rod, and the profile is a straight line. If the friction force is comparable to the elastic force, then the NW bends during manipulation. High static

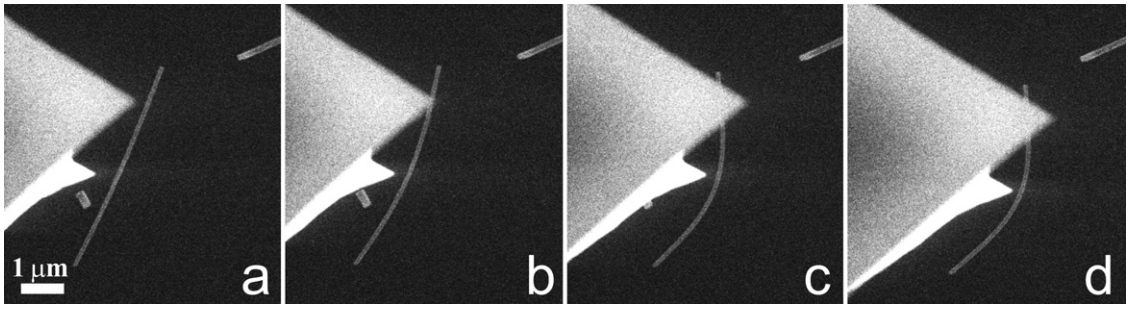

Fig. 4. Evolution of the NW shape during dragging by an AFM tip on HOPG.

friction force is able to maintain a noticeably unchanged NW profile even at the end of the manipulation.

For our experiment, a NW was dragged over several microns close to its midpoint by an AFM tip. Once the NW travels over a considerable distance (Fig. 4c), it bends into an arc due to the kinetic friction force acting along the length of the NW, and its shape remains constant during the subsequent translation. It is known that the kinetic friction force sometimes depends on the velocity of the motion [23]. Our experiments do not allow direct control of the velocity due to the stepping regime of the nanomanipulator. However, atomic friction is proportional only to logarithm of velocity at constant normal load [24]. Experiments have shown that the shape of a NW is stable during and after the drag.

We assume that the kinetic friction force q_{kin} remains constant along the length of the NW. On the other hand, the total kinetic friction force acting on the NW is balanced with the external applied lateral force. It is possible to apply the Timoshenko beam theory [25] to the NW. The elastic beam equations imply that the system remains in a state of equilibrium, i.e. it is motionless or moving uniformly. Forces of kinetic friction that have magnitudes of order 10^2 nN would produce an acceleration of order 10^{22} nm/s^2 with a NW mass of order 10^{-20} kg. Accounting for the characteristic time of the nanomanipulator system (which is much greater than 10^{-9} s), the NW would travel an estimated distance of 10^4 nm outside of the observed area during the characteristic time when deviating from equilibrium. This simple estimation concludes that the system is balanced in a nearly equilibrium state; it also allows us to consider the NW frame of reference as inertial and to apply the equilibrium equations for this case. The distributed external force f is projected onto the y-axis and affects the NW, yielding (Fig. 5a):

$$f = -q_{kin} + F_{apl-lat} \times \delta\left(l - \frac{L}{2}\right), \tag{3a}$$

where $\delta(x)$ is the Dirac delta function.The condition of zero total force implies:

$$q_{kin}L = F_{apl-lat}. \tag{3b}$$

The NW shape is thus described by a differential equation of NW equilibrium over the interval $(0, L)$ [26]:

$$IE\frac{d^2\varphi}{dl^2} = q_{kin}\left[l - LH\left(l - \frac{L}{2}\right)\right]\sin\varphi, \tag{4}$$

where E is the NW Young's modulus, I is the NW area moment of inertia, and φ is the angle between the tangent line of the NW and the direction of motion; φ is a function of the nanowire axis l and $H(x)$, the Heaviside step function. This equation can be solved numerically, and the profile obtained can be compared to the NW profiles obtained experimentally (Fig. 5).

It is worth noting that at the tip contact point, the normal component of the applied force (loading force) acts on the NW. Aside from the tip-NW contact, only the adhesion force acts as an effective normal force.

In this manner, considering the NW length, diameter, Young's modulus, and experimentally obtained shape, one can estimate the kinetic friction force. The value of the Young's modulus was measured experimentally on similar NWs. Half-suspended NWs were bent by an AFM tip attached to a quartz tuning fork force sensor inside of an SEM. In performing these experiments, we determined an average Young's modulus of 58 GPa. We determined that the magnitude of q_{kin} ranges from 0.04 to 0.5 nN/nm on HOPG (for a set of 6 NWs) and from 0.03 to 0.7 nN/nm on silicon wafers (for a set of 8 NWs). The results of distributed kinetic friction were plotted as a function of NW diameter in Fig. 6. The tendency of friction to be increasing with NW diameter is noticeable. Interfacial shear stress

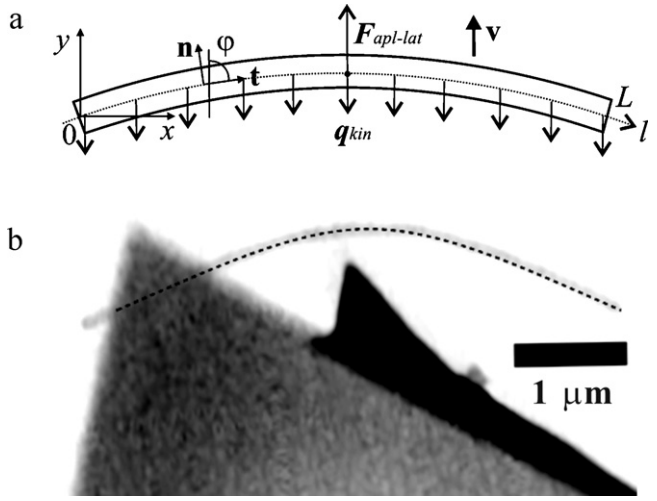

Fig. 5. A schematic of the nanowire affected by the tip applied force $F_{apl\text{-}lat}$ and the kinetic friction force q_{kin} (a). Overlay of the true SEM image of the translated NW and the calculated NW profile (dashed line). The fitting parameter for the calculated profile is the distributed kinetic friction q_{kin} = 0.04 nN/nm (b).

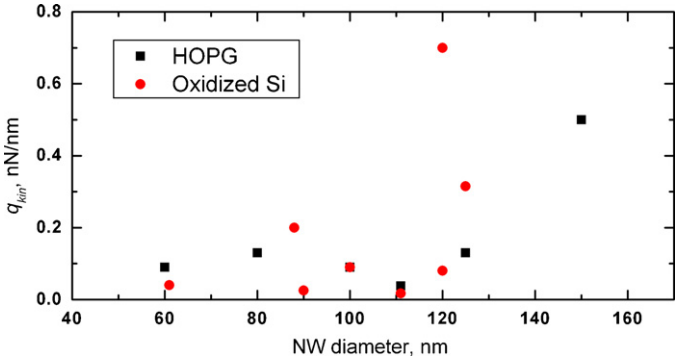

Fig. 6. Distributed kinetic friction q_{kin} as a function of NW diameter on HOPG and oxidised Si wafer.

was calculated which is a specific measure of the friction force per unit of contact area. The average shear stress is σ_{kin} = 2.75 MPa on HOPG and σ_{kin} = 3.2 MPa on silicon. Our results are comparable to the 1 MPa shear stress obtained by Manoharan for kinetic friction of ZnO NWs on silicon wafer [10].

3.3. Discussion

Variation in NW-substrate friction values is rather high in our experiment (Fig. 6). However, this problem was referred in the literature already and probably is inevitable for NWs. Conache et al. reported a variation in distributed static q_{st} greater than one order of magnitude and more than two orders of magnitude in values of the distributed kinetic friction q_{kin} for hexagonal InAs NWs [12,13]. There are several reasons for large variation in static and kinetic friction measurements. First, surface roughness or morphological defects on NW walls may cause significant effect via decreasing van der Waals (vdW) attraction force, which acts as an effective loading force and maintains friction in our experiment. The vdW force decreases due to the increasing NW-substrate distance as $F_{vdw} \sim a^{-5/2}$, where a is the distance between the NW and the substrate [27]. Second, the average value of Young's modulus was used for all NWs to determine kinetic friction. It is well known, that Young's modulus of individual ZnO nanowires may differ a lot, especially for NWs with diameters smaller than 100 nm [5,28]. Variation of kinetic friction data can be reduced significantly if the true Young modulus is used for each NW. Third, any deviation of the cross-section geometry from hexagon alters the calculated values. Employing high resolution SEM imaging can eliminate the last problem. It is possible, that NW orientation relative to the substrate may also cause friction variation (anisotropy effect) as it was demonstrated already for carbon nanotubes [22].

It is well known that static friction is commonly higher than kinetic friction for nanoscale objects [11,12,29]. The values obtained for σ_{kin} are approximately ten times less than the values obtained for σ_{com} in our experiments. We should note that σ_{kin} and σ_{com} were measured via different methods and can differ significantly. The shear stress σ_{com} is almost equal to the shear stress σ_{st} of the static friction (or at least contains a significant contribution from it), while the shear stress σ_{kin} measured during NW translation completely corresponds to the kinetic friction.

Thus, combined friction measurement method described in this article can be used for rough estimation of static friction force only. While kinetic friction measurement method produces more accurate results. However, this method only works for certain combinations of NW length, diameter, Young's modulus, and NW-substrate friction that maintain sufficient NW bending during the manipulation. The NW internal strength should be high enough to withstand the load applied by the tip during translation.

4. Conclusions

The static and kinetic frictions of ZnO NWs were studied on HOPG and oxidised silicon substrates in a vacuum at room temperature. The values of shear stress for mixed static-kinetic friction were determined to be σ_{com} = 24 MPa on HOPG and σ_{com} = 36 MPa on silicon wafers.

A new method was developed for measuring the kinetic friction of NWs on flat substrates. The method is based on profile analyses of NW bending during translation. The results generated by this method are independent of the contact geometry of the probe tip and NW; however, the NW Young's modulus must be known. The values determined for the shear stress for kinetic friction are σ_{kin} = 2.75 MPa on HOPG and σ_{kin} = 3.2 MPa on silicon wafers.

Acknowledgements

This work was supported by the Estonian Science Foundation grants 8377 and JD162, Estonian research targeted project SF0180058s07, Estonian Nanotechnology Competence Centre, and ESF Fanas program "Nanoparma". The authors are grateful to Dr. R. Kalendarev for assistance in sample preparation. The authors would like to thank Dr. E. Gnecco and Dr. K. Mougin for useful discussions.

References

[1] D. Appell, Nanotechnology: wired for success, Nature 419 (2002) 553–555.
[2] L. Samuelson, Self-forming nanoscale devices, Mater. Today 6 (2003) 22–31.
[3] W. Mai, Z. Wang, Quantifying the elastic deformation behavior of bridged nanobelts, Appl. Phys. Lett. 89 (2006) 073112.
[4] J. Song, X. Wang, E. Riedo, Z. Wang, Elastic property of vertically aligned nanowires, Nano Lett. 5 (2005) 1954–1958.
[5] R. Agrawal, B. Peng, E. Gdoutos, H. Espinosa, Elasticity size effects in ZnO nanowires – a combined experimental-computational approach, Nano Lett. 8 (2008) 3668–3674.
[6] Z. Wang, Piezopotential gated nanowire devices: piezotronics and piezophototronics, Nano Today 5 (2010) 540–552.
[7] A. Desai, M. Haque, Sliding of zinc oxide nanowires on silicon substrate, Appl. Phys. Lett. 90 (2007) 033102.
[8] Y. Zhu, Q. Qin, Y. Gu, Z. Wang, Friction and shear strength at the nanowire–substrate interfaces, Nanoscale Res. Lett. 5 (2010) 291–295.
[9] M. Manoharan, A. Desai, G. Neely, M. Haque, Synthesis and elastic characterization of zinc oxide nanowires, J. Nanomater. (2008) 849745.
[10] M. Manoharan, M. Haque, Role of adhesion in shear strength of nanowire–substrate interfaces, J. Phys. D: Appl. Phys. 42 (2009) 095304.
[11] E. Wong, P. Sheehan, C. Lieber, Nanobeam mechanics: elasticity, strength, and toughness of nanorods and nanotubes, Science 277 (1997) 1971–1975.
[12] M. Bordag, A. Ribayrol, G. Conache, L. Fröberg, S. Gray, L. Samuelson, K. Montelius, H. Pettersson, Shear stress measurements on InAs nanowires by AFM manipulation, Small 3 (2007) 1398–1401.
[13] G. Conache, S. Gray, A. Ribayrol, L. Froberg, L. Samuelson, H. Pettersson, K. Montelius, Friction measurements of InAs nanowires on silicon nitride by AFM manipulation, Small 5 (2009) 203–207.
[14] L. Dorogin, B. Polyakov, A. Petruhins, S.Vlassov, R. Lohmus, I. Kink, A. Romanov, Modeling of kinetic and static friction between an elastically bent nanowire and a flat surface, J. Mater. Res., doi:10.1557/jmr.2011.339, in press.
[15] M. Falvo, J. Steele, R.##I.I. Taylor, R. Superfine, Evidence of commensurate contact and rolling motion: AFM manipulation studies of carbon nanotubes on HOPG, Tribol. Lett. 9 (2000) 73–76.
[16] J. Hsu, S. Chang, Mechanical manipulation of hexagonal phase boron nitride nanowires on the silicon substrate utilizing Atomic Force Microscope, in: Sixth IEEE Conference on Nanotechnology IEEE-NANO, vol. 2, 2006, pp. 558–561.
[17] Z. Wang, ZnO nanowire and nanobelt platform for nanotechnology, Mater. Sci. Eng. R 64 (2009) 33–71.
[18] S. Li, C. Lee, T. Tseng, Copper-catalyzed ZnO nanowires on silicon (1 0 0) grown by vapor–liquid–solid process, J. Cryst. Growth 247 (2003) 357–362.
[19] S. Achanta, J.-P. Celis, On the scale dependence of coefficient of friction in unlubricated sliding contacts, Wear 269 (2010) 435–442.
[20] C. Ritter, M. Heyde, B. Stegemann, K. Rademann, Contact-area dependence of frictional forces: moving adsorbed antimony nanoparticles, Phys. Rev. B 71 (2005) 085405.
[21] A. Rao, E. Gnecco, D. Marchetto, K. Mougin, M. Schonenberger, S. Valeri, E. Meyer, The analytical relations between particles and probe trajectories in atomic force microscope nanomanipulation, Nanotechnology 20 (2009) 115706.
[22] M. Falvo, R. Superfine, Mechanics, friction at the nanometer scale, J. Nanopart. Res. 2 (2000) 237–248.
[23] N. Tambe, B. Bhushan, Friction model for the velocity dependence of nanoscale friction, Nanotechnology 16 (2005) 2309.
[24] E. Gnecco, R. Bennewitz, T. Gyalog, C. Loppacher, M. Bammerlin, E. Meyer, H.-J. Güntherodt, Velocity dependence of atomic friction, Phys. Rev. Lett. 84 (2000) 1172.
[25] S. Timoshenko, J. Goodier, Theory of Elasticity, McGraw-Hill Book Company, New York, 1951.
[26] L. Landau, E. Lifshitz, Theory of Elasticity, Butterworth-Heinemann, Oxford, 1986.
[27] J. Israelachvili, Intermolecular and Surface Forces, Academic Press, London, 1992.
[28] J. Song, X.Wang, E.Riedo, Z. Wang, Elastic Property of Vertically Aligned Nanowires, Nano Lett. 5 (2005) 1954–1958.
[29] D. Dietzel, M. Feldmann, H. Fuchs, U. Schwarz, A. Schirmeisen, Transition from static to kinetic friction of metallic nanoparticles, Appl. Phys. Lett. 95 (2009) 053104.